Nature Environment and Pollution Technology
An International Quarterly Scientific Journal

p-ISSN: 0972-6268
(Print copies up to 2016)
e-ISSN: 2395-3454

Vol. 25 | No. 3 | Article ID B4390 | 2026

Original Research Paper

https://doi.org/10.46488/NEPT.2026.v25i03.B4390

Open Access Journal

Clay Brick Performance with Red Mud, Waste Foundry Sand, and Silica Fume: A Taguchi Approach

Smita S. Borchate[1], Praveen A. Ghorpade[2]†, Basavaraj G. Katageri[3] and Nayana P. Hoolikantimath[4]

[1]Visvesvaraya Technological University, Belagavi, Karnataka -590018, India and Department of Civil & Environmental Engineering, Kolhapur Institute of Technology's College of Engineering (Autonomous), Kolhapur, Maharashtra-416234, India

[2]Department of Civil Engineering, KLE Technological University, Dr. M. S. Sheshgiri Campus, Belagavi-590008, Karnataka, India and Visvesvaraya Technological University, Belagavi-590018, India

[3]GITAM School of Technology, Bengaluru Campus, Bengaluru, Karnataka, India

[4]Department of Civil Engineering, KLE Technological University, Dr. M. S. Sheshgiri Campus, Belagavi-590008, Karnataka, India

†Corresponding author: Praveen A. Ghorpade; praveenghorpade1@gmail.com

Abbreviation: Nat. Env. & Poll. Technol.
Website: www.neptjournal.com

Received: 30-08-2025
Revised: 23-10-2025
Accepted: 26-10-2025

Key Words:

Red mud
Waste foundry sand
Silica fume
Clay bricks
Geopolymerisation
Grey relational analysis

Citation for the Paper:

Borchate, S.S., Ghorpade, P.A., Katageri, B.G. and Hoolikantimath, N.P., 2026. Clay brick performance with red mud, waste foundry sand, and silica fume: A Taguchi approach. *Nature Environment and Pollution Technology*, 25(3), B4390. https://doi.org/10.46488/NEPT.2026.v25i03. B4390

Note: From 2025, the journal has adopted the use of Article IDs in citations instead of traditional consecutive page numbers. Each article is now given individual page ranges starting from page 1.

ABSTRACT

This study addresses the environmental concerns associated with the disposal of red mud (RM) and Waste Foundry Sand (WFS). It explores the use of these industrial by-products, along with silica fume, fly ash, and Desur clay, to produce geopolymer clay bricks as a sustainable alternative to traditional clay bricks. Initially, 5M geopolymeric clay bricks were produced by partially substituting natural clay with RM, fly ash, WFS, sodium silicate, and caustic. The highest compressive strength achieved was 3.27 $N.mm^{-2}$ with a 5M caustic concentration. To further optimize the raw materials and enhance the strength, WFS was partially replaced with different percentages of silica fume. Grey Relational Analysis (GRA) was used to identify the most effective mix, transforming multiple objectives into a single optimal solution. Nine mix designs were developed following the Taguchi L9 orthogonal array. The optimum mix demonstrated a compressive strength of 5.02 $N.mm^{-2}$, comprising 13.75% red mud, 10% silica fume, 12.85% WFS, 33.43% Desur clay, and 30% fly ash. Water absorption remained within allowable limits across all samples. Variance analysis indicated that silica fume (47.45%) was the most influential factor, followed by red mud (30.36%), while WFS contributed the least (21.17%). Microstructural and mineralogical analyses using SEM, FTIR, and XRD confirmed the formation of geopolymeric gels and stable phases. Heavy metal assessments via ICP verified that the bricks are environmentally safe for utilization.

1. INTRODUCTION

Red mud (RM), also known as bauxite residue, is a by-product generated during Bayer's alumina production process. Globally, approximately 150 million tons of red mud are produced each year. For every ton of alumina manufactured, about 1 to 1.5 tons of red mud are generated, with the exact amount depending on the quality of the bauxite ore. The process begins with the fine grinding of bauxite ore using a ball mill in a wet environment. The resulting slurry is then digested in a caustic solution, dissolving the alumina while leaving behind solid red mud. This red mud is separated after several washing steps. The high pH (11–13) of the residue is mainly due to residual caustic bound to the red mud. Land disposal and lagooning methods can lead to groundwater contamination through alkali leachate. Conversely, dry stacking can cause airborne pollution because of the fine particles. Both disposal methods require significant land area, making them costly and environmentally challenging (Rai et al. 2020).

Early research showed the use of processed red mud as a material for road construction and the stabilization of acidic soil (Reddy et al. 2021). Red mud is

also utilized as a partial substitute for fly ash, cement, and filler material. Bricks or blocks made with stabilized red mud using 5% hydrated lime can be used to construct the walls of economical dwellings (Dass & Malhotra 1990, Kumar et al. 2021).

Waste Foundry Sand (WFS) is another industrial solid waste of concern, generated after becoming worn out during mold-making in metal casting industries. Foundry sand, along with binders, is frequently used for casting molds. After repeated use, the foundry sand becomes unsuitable for new molds. Such sand is termed WFS (Matos et al. 2019). Several authors have studied its use as a replacement for natural sand and Portland cement in concrete, as well as a replacement for fine aggregate to improve strength. Some researchers have explored using 30% WFS to replace natural sand in the production of clay bricks. The utilization of WFS remains a challenge despite its various applications (Billong et al. 2021, Matos et al. 2019).

Silica fume (SF) is a by-product generated during the production of silicon and ferrosilicon alloys. Its main component is non-crystalline silica (SiO_2), constituting approximately 85 to 99% of the material. Silica fume is primarily used in various construction and industrial applications, including concrete and grout for parking decks, marine structures, and highway bridges, as well as in oil well cementing, cementitious restoration products, and refractory and ceramic materials (Siddique & Chahal 2011).

Recycling industrial waste such as red mud, waste foundry sand, fly ash, and silica fume promotes green construction by reducing pollution, conserving natural resources, and minimizing landfill use. This approach creates eco-friendly materials, improves resource efficiency, and supports a circular economy while aligning with global sustainability goals (Kumar et al. 2025). Environmental regulations have become more restrictive regarding the safe disposal of these wastes. Due to the growing demand for bricks as a construction material, many researchers have attempted to utilize wastes such as fly ash, sludge, wood sawdust, processed waste tea, rubber, polystyrene, waste glass, acrylic waste, and limestone dust in the manufacture of conventional burnt clay bricks (Ishaq et al. 2025, Saravanan & Rao 2023).

Mineral deposits such as clay soil are extensively used to manufacture conventional burnt clay bricks. Asia produces approximately 1.2 trillion clay bricks per year. About 75% of the world's clay bricks are manufactured in China, India, Pakistan, and Bangladesh. India's annual utilization of burnt clay bricks is 180 billion tons (Abbas et al. 2017). It is estimated that 350 million tons of fertile topsoil are used every year to make burnt clay bricks. To overcome the issues associated with conventional burnt clay bricks, such as greenhouse gas emissions, high-temperature processing, and reduced productivity of surrounding fertile land, the Government of India has prohibited the production of clay bricks and promoted alternative building materials (Hafez et al. 2022).

Bottom ash (F-class), when combined with a highly alkaline solution, can be used as a pozzolanic material. It produces an aluminosilicate polymer through a chemical reaction, known as a geopolymer. Apart from reducing the cost of conventional bricks, the production of geopolymeric clay bricks derived from fly ash facilitates the utilization of industrial waste (Nandipati et al. 2023). Most studies have used sodium silicate and sodium hydroxide as activators for producing geopolymeric fly ash-based bricks (Bajpai et al. 2020, Turkey et al. 2022). Considering the disposal problems associated with red mud due to its alkalinity, various efforts have been made to neutralize it. However, the neutralization of red mud would be uneconomical (Phoo-ngernkham et al. 2014).

Red mud has proven effective as a geopolymer composite binding material, along with metakaolin, fly ash, coal gangue, slag, arsenic sludge, and rice husk (Apithanyasai et al. 2020, Mudgal et al. 2021). Geopolymers consist of Si and Al tetrahedra linked with oxygen atoms in the three-dimensional structures of Calcium Silicate Hydrate (C-S-H) and Sodium Aluminosilicate Hydrate (N-A-S-H) gel. The strength of this network depends on the soluble silicon dioxide and aluminum oxide from the aluminosilicate materials. Silicon dioxide from fly ash readily dissolves through alkali ions, but alumina from red mud dissolves more slowly. Since silica fume contains a high amount of amorphous SiO_2, its use with other aluminosilicate components increases the Si/Al ratio in the geopolymer system. Geopolymer strength is positively affected by an increased molar ratio because more sodium aluminosilicate hydrate gel (N-A-S-H) is formed. The finer particle size of silica fume provides a large surface area and accelerates the reaction between the alkaline activator and aluminosilicate materials. These properties of silica fume are beneficial in enhancing the geopolymer reaction (Sutar et al. 2014).

Initially, bricks were cast using WFS and fly ash with alkaline activators, namely sodium silicate and sodium hydroxide, at two different concentrations: 10M and 12M. For bricks prepared with 12M caustic concentration, the highest compressive strength of 3.5 $N.mm^{-2}$ with 3.93% water absorption was achieved. However, these bricks showed strong efflorescence. To overcome this problem, the caustic concentration was lowered to 5M. However, the strength of these bricks was 3.27 $N.mm^{-2}$ (Gaonkar et al.

2023). Therefore, it is important to improve the compressive strength while maintaining a 5M caustic concentration. The present work explores the effective use of silica fume and red mud to increase compressive strength.

According to the conventional procedure, multiple experiments are needed to determine the effect of different percentages of RM, SF, and WFS on the compressive strength of red mud-based geopolymeric bricks (Mohmed & Scholar 2018, Sutar et al. 2014, Rajesrajeswari et al. 2014). An appropriate trial design was required to minimize the number of experiments and evaluate the effects of individual constituents. The Taguchi method is an effective approach for designing experiments with the fewest trials (Rai et al. 2012). The Taguchi multi-response Grey Relational Analysis (GRA) method can also identify the best set of factor values for multiple responses simultaneously (Shivaprasad & Das 2018).

While numerous studies have investigated the use of industrial wastes in brick manufacturing, a significant knowledge gap persists in the area of comprehensive multi-response optimization, particularly through the integrated application of Taguchi and Grey Relational Analysis (GRA) for systems involving multiple waste materials. This study addresses that gap by employing a structured Taguchi–GRA approach to optimize the combined influence of RM, SF, and WFS in clay-based brick formulations. The primary objective of the present work is to determine the optimal mix parameters that achieve a balance between mechanical strength and water absorption under varying proportions of waste inputs. The findings highlight the effectiveness of multi-response optimization in enhancing waste valorization, offering a viable pathway for large-scale industrial reuse of hazardous and non-biodegradable wastes. This work supports sustainable construction practices by minimizing reliance on natural clay, improving environmental safety, and advancing circular economy principles within the building materials industry.

2. MATERIALS AND METHODS

2.1. Materials

The materials used for making bricks included fly ash (Class F, JSW Energy Ltd., Ratnagiri, Maharashtra, India), red mud (HINDALCO Industries Ltd., Belgaum, Karnataka, India), waste foundry sand (Aqua Alloys Pvt. Ltd., Shinoli, Maharashtra, India), and silica fume (Cilantro Chemicals Pvt. Ltd., Navi Mumbai, Maharashtra, India). These materials had a particle size of less than 45 μm, with content below 2.0%, a specific surface area of over 19 $m^2.g^{-1}$ as measured by Brunauer-Emmett-Teller (BET) analysis, and bulk density ranging from 500 to 700 $kg.m^{3-}$. Additional materials included clay from Desur, Belagavi, Karnataka, India. The chemicals utilized were sodium hydroxide pellets (NaOH, Nice Chemicals LR grade, 97% purity), sodium silicate (Na_2SiO_3, Sunchem Chemicals, containing 16.25% Na_2O, 34.25% SiO_2, and 49.50% water), and demineralized water (conductivity < 10 $\mu S.cm^{-1}$).

2.2. Methodology for Casting Various Combinations of 5M Red Mud Bricks Using A Geopolymeric Approach

Initially, screening experiments with 5M geopolymeric clay bricks involved partially replacing natural clay with RM (18.79%), fly ash (30%), WFS (22.85%), sodium silicate, and caustic. The highest compressive strength achieved was 3.27 $N.mm^{2-}$. To optimize raw materials and enhance the strength of 5M bricks, a portion of the WFS was substituted with various percentages of silica fume, and experimental design and analysis were performed using GAG.

2.2.1. Experimental Method

Standard-size clay bricks measuring 230 mm X 110 mm X 70 mm were cast using a hydraulic-press brick-making machine operating at 13 MPa, following a geopolymeric approach. The raw materials were mixed with geopolymeric constituents, including sodium silicate and sodium hydroxide,

Table 1: Different material weight percentages used in various sets of geopolymer bricks in the present study.

Set of bricks	RM [%]	SF [%]	WFS [%]	FA [%]	Molarity from fresh Caustic	Molarity of Caustic from Red mud
A	13.75	5	17.85	30	4.09	0.91
B	13.75	10	12.85	30	4.09	0.91
C	13.75	15	7.85	30	4.09	0.91
D	18.79	5	12.38	30	3.75	1.25
E	18.79	10	7.85	30	3.75	1.25
F	18.79	15	17.85	30	3.75	1.25
G	23.79	5	7.85	30	3.42	1.58
H	23.79	10	17.85	30	3.42	1.58
I	23.79	15	12.85	30	3.42	1.58

at a ratio of 2.5 to produce different sets of bricks, as shown in Table 1.

All raw materials, including Desur clay, waste foundry sand (WFS), fly ash, silica fume, and red mud, were initially dry-mixed to achieve uniform distribution. Water and the alkaline activator were then added to form the geopolymer mixture. Red mud containing bound caustic was partially substituted for fresh caustic to minimise the risk of caustic leaching from the cast bricks. The Na_2O content in red mud indirectly represents the amount of bound caustic available within it.

The cast bricks were first cured at room temperature for 24 h. To accelerate the geopolymerisation process, the partially dried bricks were subsequently heat-cured in an oven at 80°C for another 24 hours. After heat curing, the bricks were removed and wrapped in a wet cloth for six days under ambient conditions. The curing regime plays a crucial role in determining both the rate and extent of geopolymer formation. Elevated temperatures, such as 80°C, enhance the dissolution of reactive silica and alumina species, thereby accelerating the chemical reactions responsible for geopolymer bond formation. The subsequent moist curing phase supports structural stabilisation and contributes to gradual strength development.

Variations in curing temperature and duration significantly influence the reaction mechanisms, phase evolution, and overall mechanical performance of the geopolymeric matrix. Geopolymers consist of three-dimensional silicoaluminate networks formed by interconnected silicon and aluminium tetrahedra linked through oxygen atoms. While the amorphous silica present in fly ash readily dissolves in the alkaline activator, only limited alumina dissolves from red mud under ambient conditions. Therefore, elevated temperature is essential to facilitate the dissolution of Al^{3+} ions from red mud, enabling its effective participation in the polycondensation process and contributing to the formation of a stronger geopolymeric structure.

The prepared bricks were further evaluated for compressive strength and water absorption. These properties were measured following the standard procedures outlined in IS 3495:1992 (Parts 1 and 2). To investigate the microstructural and mineralogical characteristics of the bricks, X-ray diffraction (XRD), scanning electron microscopy (SEM), and Fourier Transform Infrared Spectroscopy (FTIR) analyses were conducted.

The XRD analysis was performed using a Rigaku SmartLab diffractometer, with a scanning range of 2θ from 5° to 90° at a constant scanning speed of $1°.min^{-1}$, employing CuKα radiation (λ = 1.540 nm). The diffraction peaks obtained were identified and matched with the standard reference database of the Joint Committee on Powder Diffraction Standards (JCPDS) to determine the crystalline phases present in the samples.

The morphological features and surface characteristics of the bricks were examined using a Scanning Electron Microscope (MIRA3 LMH, TESCAN, Brno, Czech Republic, EU). In addition, FTIR analysis was carried out using a BRUKER-ALPHA 100508 Fourier Transform Infrared spectrophotometer to identify the functional groups and bonding environments within the geopolymeric matrix. The spectra were recorded over a wavenumber range of 4,000-400 cm^{-1}.

To assess the environmental stability of the developed bricks, leachate analysis was conducted to determine the potential release of heavy metals. Microwave-assisted acid digestion was performed according to EPA SW-846 Methods 1311 and 3015. For this purpose, the brick samples were crushed into fine powder and passed through a 90 µm sieve to ensure uniform particle size. The powdered samples were pre-digested overnight in 5 mL of nitric acid, followed by the addition of 10 ± 0.1 mL of concentrated nitric acid. The digestion process was carried out in a microwave digester at 175°C for 30 minutes, with the sample vessels rotated at 30 rpm to ensure consistent heating and reaction.

After digestion, the vessels were allowed to cool, and the resulting solutions were filtered to remove any remaining particulates. The filtrates were then transferred into volumetric flasks and diluted to a known volume using demineralised water. The prepared samples were subsequently analysed for heavy metal concentrations using Inductively Coupled Plasma (ICP; MY15230013, Software Version: 7.3.0.8799, Firmware Version: 3354). This analysis provided insight into the leaching behaviour and environmental safety of the geopolymer bricks.

2.2.2. Multi-Response Optimization, Grey-Based Taguchi Method

The Taguchi orthogonal design approach was employed for casting the red mud-based geopolymeric bricks. Three parameters, RM, SF, and WFS, were selected as variables for this study. The fly ash content was kept constant at 30%. The percentage of Desur clay varied with respect to red mud. The ranges and parameter levels were selected based on earlier screening work conducted during the preparation of geopolymeric bricks (Gaonkar et al., 2023). A Taguchi array is called an orthogonal array, where one of the parameters is tested at each level. The L9 orthogonal array, which contains three factors and three levels in the Taguchi method, was employed for the experiments listed in Table 2. In total, nine experiments were carried out. The compressive strength and water absorption values were

Table 2: Factors and levels.

Factors	Level 1[%]	Level 2[%]	Level 3[%]
RM	13.75	18.79	23.79
SF	5	10	15
WFS	17.85	12.85	7.85

obtained from triplicate samples, denoted as Y1, Y2, and Y3 for compressive strength, and W1, W2, and W3 for water absorption, respectively. These values were obtained for each experiment in the L9 array, as shown in Table 3. For the design to work, eight degrees of freedom (DOF) were required.

2.2.3. *Optimisation Steps for Grey-Based Taguchi Method*

The following steps were carried out to optimize factors using the Grey-based Taguchi method. Additionally, these steps are demonstrated with a flowchart as shown in Fig. 1.

Step I: Calculation of Signal-to-Noise Ratio (S/N)

To work out the S/N ratio for every response, the following equation was used:

i. Larger-the-better

$$\text{S/N ratio} = -10 \log_{10}\left(\frac{1}{k}\sum_{i=1}^{n}\frac{1}{x_{ij}^2}\right) \quad \ldots(1)$$

where k = number of replications and xij=observed response value, where i=1, 2, ...m, j=1, 2, ...n. This is used in experiments where maximization of the quality characteristic is required. This is suggested to be the larger-the-better type of experiment.

ii. Smaller-the-better

$$\text{S/N ratio} = -10 \log_{10}\left(\frac{1}{k}\sum_{i=1}^{n} x_{ij}^2\right) \quad \ldots(2)$$

This is designated the smaller-the-better type experiment, where minimization of the characteristic is required.

Step II: Normalization of S/N ratio.

Normalization is modifying a single data input to distribute the data uniformly and scale it into a suitable range for further analysis. The original data must be standardized using the following formula before applying the grey relation theory to the analysis. A suitable value is subtracted from the values in the same array to estimate the value of this array. Use the S/N ratio value when normalizing data for a grey relation analysis.

(To be used for S/N ratio, with the Larger the better manner)

$$Zij = \frac{y_{ij} - min(y_{ij}, i=1,2,\ldots\ldots n)}{max(y_{ij}, i=1,2,\ldots\ldots n) - mi \;\; (y_{ij}, i=1,2,\ldots\ldots n)} \quad \ldots(3)$$

(To be used for S/N ratio, with the smaller the better)

$$Zij = \frac{max y_{ij}, i=1,2,\ldots\ldots n) - y_{ij}}{max(y_{ij}, i=1,2,\ldots\ldots n) - min(y_{ij}, i=1,2,\ldots\ldots n)} \quad \ldots(4)$$

*S*tep III: Calculation for absolute difference (Δ)

$$CG_{ij} = \frac{\Delta_{min} + \lambda \Delta_{max}}{\Delta_{ij} + \lambda \Delta_{max}}, \quad \ldots(5)$$

Step IV: Calculation of the Grey Relational Coefficient (GC)

$CG_{ij} = \frac{\Delta_{min} + \lambda \Delta_{max}}{\Delta_{ij} + \lambda \Delta_{max}}$ where λ= Distinguishing coefficient in the range $0 \leq \lambda \leq 1$ …(6)

The distinguishing coefficient was assigned a value between zero and one based on the responses.

Step V: Generate the Grey Relational Grade (GRG)

$$GRG = \frac{1}{m}\sum CG_{ij} \quad \ldots(7)$$

Where CG_i is the Grey Relational Grade for the j^{th} response and m is the number of performance factors.

Table 3: L9 Orthogonal array for factors and responses.

Set No.	RM [%]	SF [%]	WFS [%]	Responses					
				Compressive Strength [N.mm^{-2}]			Water Absorption [%]		
				Y1	Y2	Y3	W1	W2	W3
A	1	1	1	3.68	3.01	3.47	12.20	12.0	12.39
B	1	2	2	5.41	4.45	5.20	16.05	14.88	13.91
C	1	3	3	3.76	4.60	4.49	15.18	15.46	13.34
D	2	1	2	3.64	3.63	3.42	14.95	11.95	13.95
E	2	2	3	3.10	3.10	3.09	12.20	11.95	12.41
F	2	3	1	3.65	3.44	3.30	11.90	12.10	12.53
G	3	1	3	2.49	2.72	2.48	12.29	13.17	12.30
H	3	2	1	3.10	3.14	3.15	13.57	14.81	13.41
I	3	3	2	3.47	3.50	3.11	14.02	13.17	12.43

Step VI: Calculation for optimal factor and its level combination.

A factor level total table was prepared based on the GRG value for all factors and levels.

Step VII: Execute analysis of variance (ANOVA) to obtain a significant factor.

To perform ANOVA, the following steps were used:

Total variation

$$SS_T = \sum_{i=1}^{n} GRG_i^2 \; - \; CF \qquad \ldots(8)$$

Where,

CF = Correction Factor

$$CF = \frac{\sum_{i=1}^{n} GRG^2}{Total\ no.of\ experiment} \qquad \ldots(9)$$

a. The variation (S) for each factor and level was calculated using the same formula.

b. The Degree of Freedom (DOF) was calculated.

c. The individual degree of freedom was calculated by subtracting the number of levels.

d. Calculation of Error

e. The variance value (V) and the F value were calculated,

$$V = \frac{S}{DOF} \qquad \ldots(10)$$

f. The percentage of the Contributing Factor (%CF).

3. RESULTS AND DISCUSSION

In the present study, geopolymeric bricks were cast using red mud, silica fume, WFS, Desur clay, and a constant 30% fly ash. The main constituents of red mud were Fe_2O_3 and Al_2O_3. At the same time, Desur clay contained CaO, K_2O, SiO_2, and Al_2O_3 as its major constituents. Silica fume contained the highest amount of SiO_2 (92%). WFS also consisted primarily of SiO_2 as a major constituent, the composition of which is presented in Table 4. The XRD patterns of these materials are shown in Fig. 2. The minerals identified in the XRD patterns and the XRF oxide compositions presented in Table 4 are in alignment. The raw materials used in the present study were selected such that their oxide compositions play a significant role in the formation of minerals responsible for imparting strength to the clay bricks.

3.1. Compressive Strength and Water Absorption

The subsequent segment addresses the effect of the varied

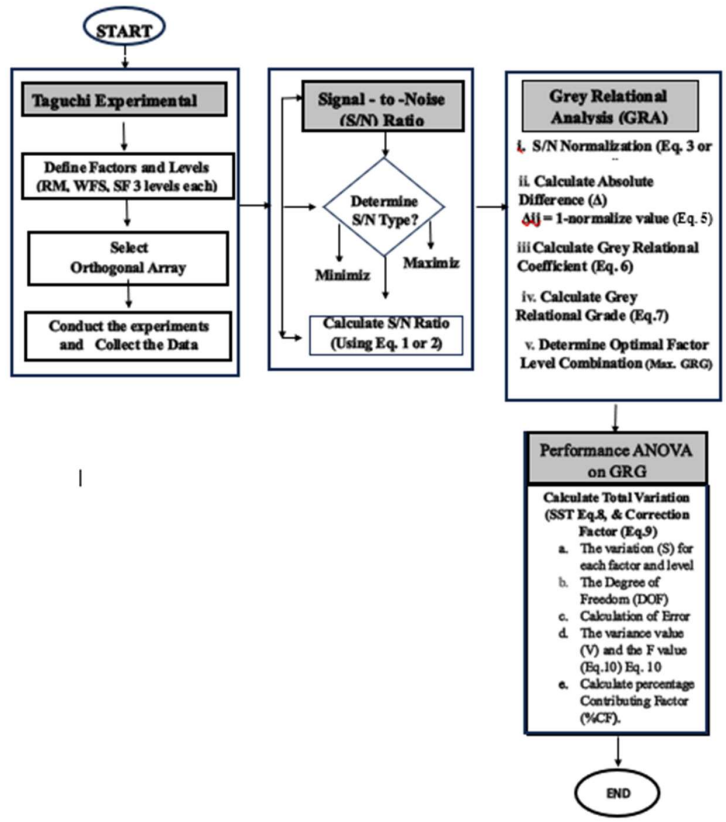

Fig. 1: Flowchart to optimize factors using the Grey-based Taguchi method.

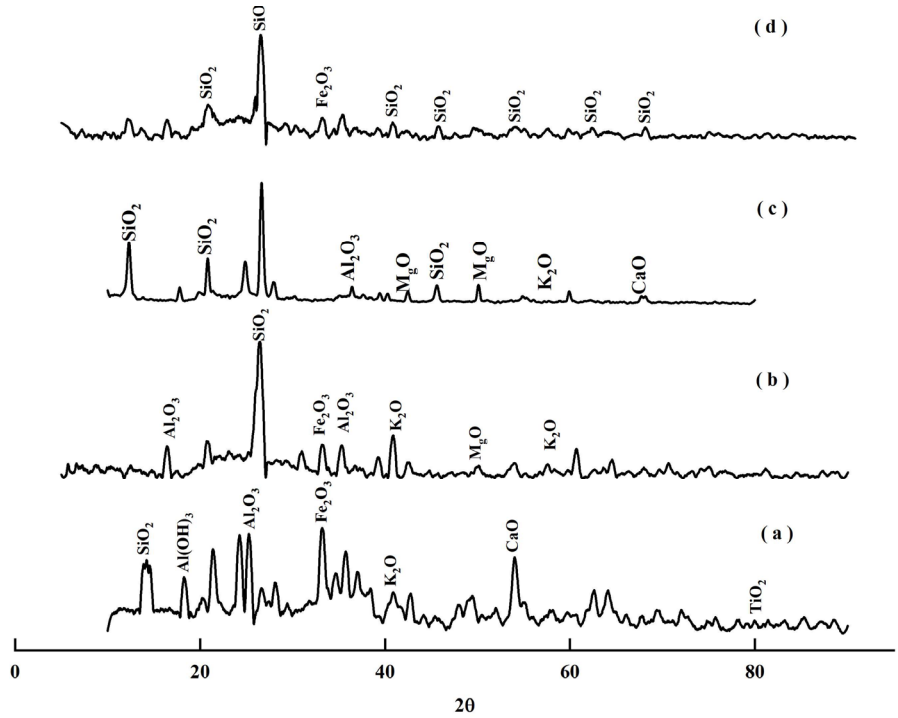

Fig. 2: XRD plot of (a) RM, (b) Fly ash, (c) Desur clay, and (d) SF.

Table 4: XRF of raw materials used in the present study.

Name of raw material	Oxide Composition % (w/w)													
	SiO_2	Al_2O_3	Fe_2O_3	Na_2O	CaO	TiO_2	P_2O_5	V_2O_5	Mn_2O_3	MgO	K_2O	MnO	Moisture	LOI
RM	10.84	20.80	39.99	5.89	3.23	6.90	0.318	0.25		-	-	-	21.40	10.6
Desur clay	57.74	28.37	8.04	0.85	0.61	1.04	0.06	-		0.64	2.44	0.03		0.08
WFS	87.91	4.70	0.94	-	0.14	0.15	-	-	0.25	0.30	0.25			5.15
SF	92.0	-	<1.0	<0.1	-	-	-	-		-	-	-	-	<3.0
Fly ash	SiO_2+ Al_2O_3+ Fe_2O_3			SiO_2	Reactive silica		SO_3	MgO	Cl					LOI
	92.3			61.34	31.11		0.01	1.01	<0.01					0.63

weight fractions of RM, SF, and WFS on the geopolymer matrix's strength, water absorption, and microstructure in different brick sets.

3.1.1. Mineralogical Characterisation

The bricks with maximum compressive strength in each set, namely brick B from sets A, B, and C, Brick D from sets D, E, and F, and brick I from G, H, and I, were selected for studies. The raw materials in the present work were selected such that their oxide compositions play a significant role in forming sodium aluminum silicate and sodium aluminum silicate hydroxide, the geopolymeric minerals responsible for giving strength to the 5M geopolymeric clay bricks. Due to the formation of these minerals, 5 M cast bricks gain a maximum compressive strength of 5.02 $N.mm^{2-}$ as compared to the control bricks (traditional clay bricks), which are composed of two different types of clays along with carbonaceous ash and calcined at more than 1000 °C, whose compressive strength was 3.5 $N.mm^{2-}$.

Set B gave the highest compressive strength, and Desur clay contributes both aluminum oxide and potassium oxide, positively affecting compressive strength. Fly ash is also a source of aluminum oxide. SF is a source of reactive silica. The optimum combination of these constituents could lead to the formation of potassium sodium aluminum silicate, sodium aluminum silicate, and calcium silicate hydrate (C-S-H) as summarised in Table No. 5). The formation of potassium sodium aluminum silicate was seen at 2Θ values

Table 5: Minerals contributing to strength for brick sets B, D and I.

2Θ	Name of mineral	Phase	Contribution to strength
20.8	Potassium sodium aluminum silicate	-	Positive
26.6			
40.81			
42.42			
59.9			
27.56	Sodium aluminum silicate	N-A-S	Positive
35.50	Sodium aluminum silicate hydroxide	N-A-S-H	Positive
54.86			
29.39	Calcium Silicate Hydrate	C–S–H	Positive
30.27			
39.42			

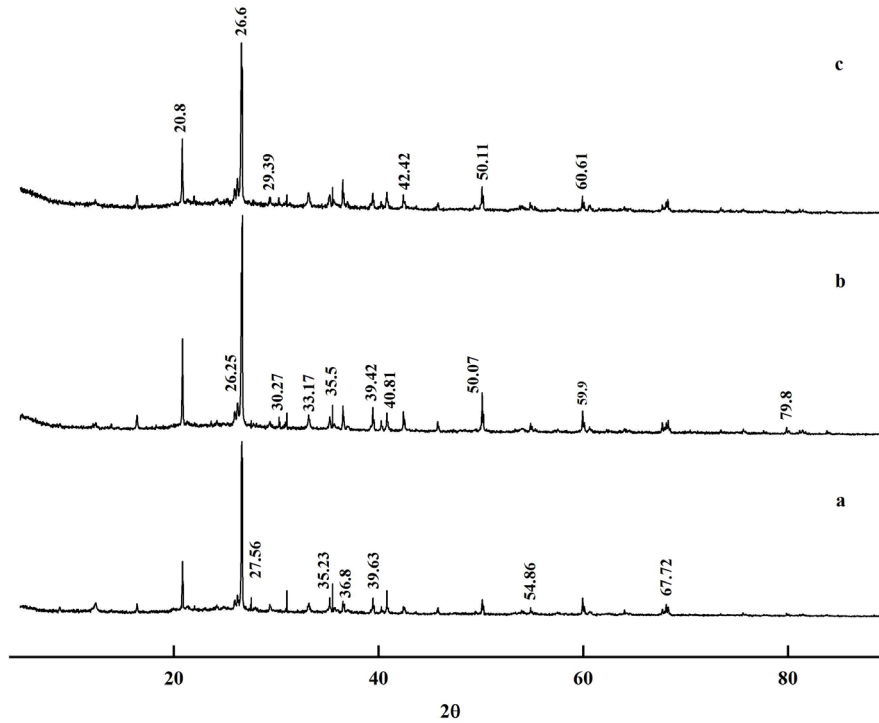

Fig. 3: XRD Analysis of (a) set B, (b) set D, and (c) set I bricks.

of 20.8, 26.6, 40.81, 42.4 and 59.9 (JCPDS-860683), sodium aluminum silicate at 2Θ value of 27.56 (JCPDS-831618), sodium aluminum silicate hydroxide at 2Θ values of 35.5 and 54.86 (JCPDS-832129) and C-S-H at 29.39, 30.27, 39.4 and 60.61 (JCPDS-722396).

The peak of sodium aluminum silicate was attributed to the compressive strength of the brick by forming the N-A-S-H. Using red mud and activated fly ash in geopolymeric processes, researchers have proven the formation of sodium aluminum silicate and sodium aluminum silicate hydroxide geopolymeric minerals. (Apithanyasai et al. 2020). These minerals are responsible for strength. The intensity for these peaks was highest in set B bricks compared to sets D and I. The area under the respective peak value of these minerals was calculated for this set of bricks. The peak area under respective peak values for these minerals is shown in Table 6.

The area under these peaks also indicated that set B had the highest peak area of these minerals compared to sets D and I. All these minerals discussed above are known to contribute to the compressive strength of the bricks. The minor peaks of SiO_2 were seen at 2θ values of 26.25, 39.63,

Table 6: Area under the peak for brick sets B, D and I.

Name of mineral	2Θ	Area under the peak for each set		
		Set B	Set D	Set I
Potassium sodium aluminum silicate	20.8	649.32	481.36	167.7
	26.6	1238.76	435.4	417.54
	40.81	224.01	173.98	101.41
	42.42	505.33	307.55	224.01
	59.9	187.0	84.82	79.98
Total area		2804.42	1483.11	990.64
Sodium aluminum silicate	27.56	87.88	25.46	23.45
Total area		87.88	25.46	23.45
Sodium aluminum silicate hydroxide	35.50	227.77	91.09	257.76
	54.86	425.36	58.50	90.25
Total area		**653.13**	**149.59**	**348.01**
Calcium Silicate Hydrate	29.39	461.1	51.16	131.41
	30.27	461.1	113.58	82.48
	39.42	134.56	131.41	114.04
	60.61	209.66	157.83	155.11
Total area		**1266.42**	**453.98**	**483.04**

50.07, and 79.8, matching with JCPDS card no. 870703 in all the brick sets.

The compressive strength results of different brick combinations are demonstrated in Fig. 4. Bricks set A, B, and C had 13.75% red mud, such that 0.91M of caustic from red mud contributed to the total caustic concentration of 5M. The compressive strength for sets A, B, and C was 3.38 N.mm^{-2}, 5.02 N.mm^{-2}, and 4.28 N.mm^{-2}, respectively.

The second set of bricks, D, E, and F, was cast similarly to the above, except the percentage of red mud increased from 13.75% to 18.79%, contributing to 1.25M of caustic associated with red mud. On the other hand, the caustic from sodium hydroxide was reduced to 3.75M to get a total molarity of 5M. Compressive strength of 3.46 N.mm^{-2} for brick set F, 3.1N.mm^{-2} for set E, and 3.56 N.mm^{-2} for set D were obtained.

The third set of bricks, G, H, and I, comprised 23.79% red mud, so 1.58 M of caustic from red mud contributed to the total caustic concentration of 5M. The compressive strengths for brick sets G, H, and I were 2.57 N.mm^{-2}, 3.13 N.mm^{-2}, and 3.36 N.mm^{-2}, respectively.

The first set of bricks, A, B, and C, gave maximum mean compressive strength compared to the second and third brick sets. The fresh caustic and aluminum oxide concentrations were highest in the first set. Desur clay contributes to both aluminum oxide and potassium oxide, and it induces a positive effect in gaining compressive strength. Fly ash was also a source of aluminum oxide. SF was the source of reactive silica. The optimum combination of such constituents could lead to the formation of sodium

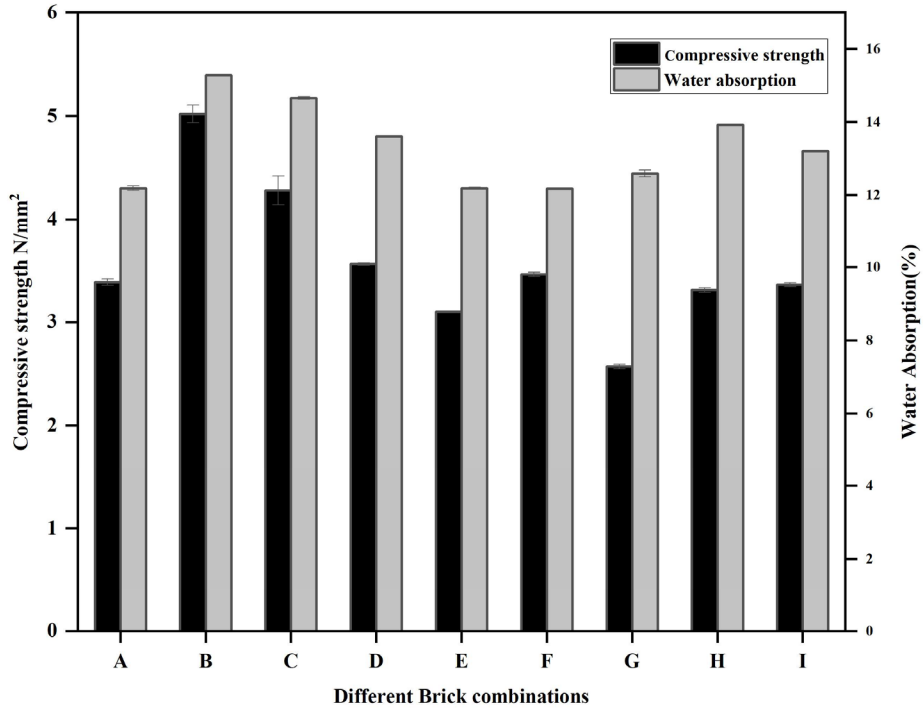

Fig. 4: Compressive strength and water absorption for different brick combinations.

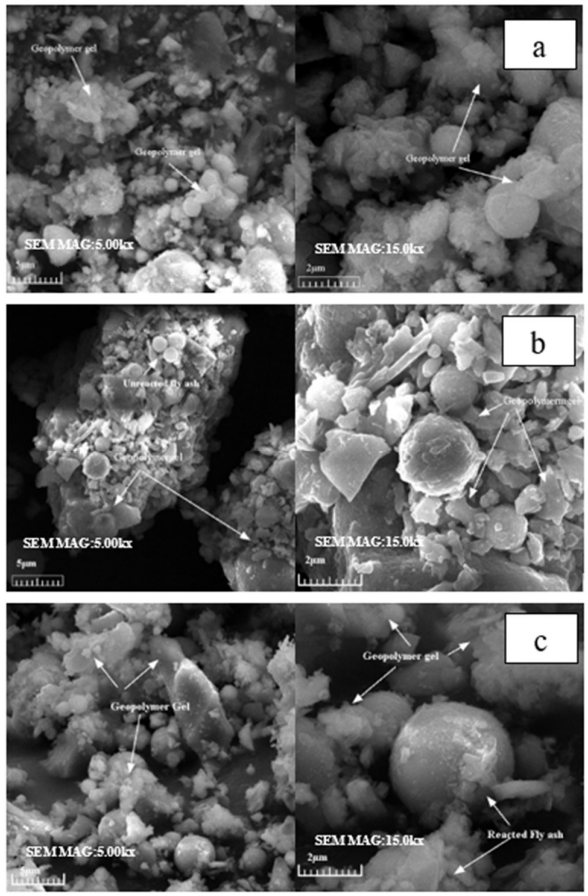

Fig. 5: SEM micrograph of (a) set B, (b) set D and (c) set I bricks. (Magnification 5000 x and 15000 x).

aluminum silicate, calcium silicate hydrate, and potassium sodium aluminum silicate. The composition of these minerals is highest in the B set of bricks, which resulted in maximum compressive strength. Further, to confirm the formation of these minerals, an XRD study was performed with sets B, D, and I bricks. The cast bricks B, D, and I gained the maximum compressive strength as compared to other brick combinations. The B set of bricks was cast with 10% SF, the D set of bricks was cast with 5% SF, and the I set was cast with 15% silica fume. Among these three sets of bricks, the maximum compressive strength of 5.02 $N.mm^{-2}$ (set B) was achieved compared to 3.56 (set D) and 3.36 (set I). These results clearly demonstrate that the optimal percentage of SF is important in strength reactions. If we reduce the percentage of SF from 10% to 5%, its compressive strength reduces from 5.02 $N.mm^{-2}$ to 3.56 $N.mm^{-2}$, and if we increase it to 15 %, its compressive strength reduces to 3.36 $N.mm^{-2}$. Fig. 4 shows that all the brick sets passed the water absorption test, which varied between 11% and 15% and is acceptable as per IS1077:1992 standards. The dense polymeric minerals formed could fill the microscopic voids, resulting in less water absorption.

3.1.2. Scanning Electron Microscopy (SEM) Analysis

The SEM analysis is shown in Fig. 5 for brick sets B, D, and I. In set B (Fig. 4a), when 10% silica fume was used, there were fewer fly ash particles, and the matrix looked denser than in sets D and I. In addition to sodium aluminum silicate hydrate gel, calcium silicate hydrate and calcium aluminum silicate hydrate gels are also produced by fly ash and silica fume geopolymer reaction. The earlier researchers (Phoo-ngernkham et al. 2014) or calcium aluminum silicate hydrate. The inorganic polymer formed within set B (Fig. 5a) is continuous and denser than that in set D, leading to higher compressive strength. The unreacted silicon dioxide and aluminum oxide in fly ash and RM are embedded in the geopolymer gel phase to form a more homogeneous and dense structure. Brick sets D, and I had reduced compressive strength due to a huge quantity of unreacted fly ash and RM particles. As a result, loose and porous geopolymer gel forms, as seen in Fig. 5(b, c). Similar outcomes were reported in other literature (Shivaprasad & Das 2018).

3.1.3. Fourier Transform Infrared Spectrometry (FTIR) Analysis

Fig. 6 (a-c) illustrates the FTIR spectra of brick sets B, D, and I. The absorption bands at 3697 cm^{-1} and 3617 cm^{-1} are assigned to the vibration of the O-H mode (Sontia Metekong et al. 2024). The H-OH bending vibration is represented by the bands between 1600 cm^{-1} and 1650 cm^{-1} in all three sets of bricks. Previous researchers reported similar spectra. (Shill et al. 2020). The FTIR spectra at 1081.34 cm^{-1}, 1082.55 cm^{-1}, and 1082.37 cm^{-1} are allied for asymmetrical elastic oscillation regions of Si-O-Al or Si-O-Si. Earlier researchers have reported similar stretching (Ogundiran & Kumar 2015). Similarly, Si-O-Si vibrations were seen at 1089.16 cm^{-1} and 1081 cm^{-1}. Spectra linked to around 465 cm^{-1} and 469.0 cm^{-1} indicate symmetric stretching and O-Si-O bending vibrations. The formation of O-Si-O (465 cm^{-1}) or Si-O-Al (1080 cm^{-1}) due to dissolution of silica from SF and alumina from RM when it comes in contact with alkaline activator at elevated temperature(80°C) during the polycondensation process (Bajpai et al. 2020).The Si-O-Al bending vibration at 555 cm^{-1}, 545.5 cm^{-1}, and 790 cm^{-1} bonds of an inorganic polymer chain in all brick sets when red mud is present. The previous study reported the same finding (Jozanikohan & Abarghooei 2022, Toniolo et al. 2017). Sodium aluminum silicate gel at peak positions 35.5 and 54.86, as shown in XRD analysis (Fig.3), is due to the geopolymeric reaction of silicate and aluminum oxide originating from fly ash and red mud. The stretching can be correlated to the dissolution of SiO_2 and Al_2O_3.

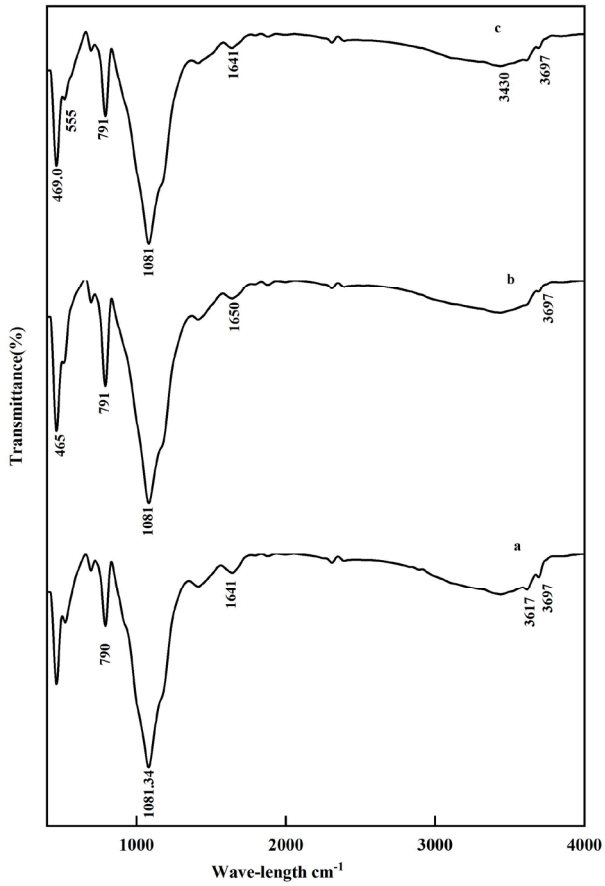

Fig. 6: FTIR Analysis of (a) set B, (b) set D and (c) set I cast red mud-based geopolymeric bricks.

3.1.4. Heavy Metal Leaching from Geopolymeric Bricks Composed of Red Mud

The geopolymeric bricks labeled B, D, and I were subjected to leaching tests for heavy metals. The testing followed the EPA protocols outlined in SW-846 methods 1311 and 3015 to assess toxicity. The results, presented in Table 7, show that all elements have leachability levels below the maximum limits established by the United States Environmental Protection Agency (USEPA), based on microwave-assisted acid digestion procedures. However, aluminum and sodium were found to leach from these bricks. Similar findings are reported in existing literature. The geopolymerization process may not fully incorporate all aluminum into a stable polymeric network, leaving some aluminum in a more reactive state. This residual reactivity can lead to aluminum leaching. The geopolymer matrix depends on sodium ions to balance the negative charge of the aluminosilicate framework. Yet, some sodium ions are only weakly bound and can be leached out when exposed to water (Kumar & Kumar 2013, Duxson et al. 2007).

Table 7: The amount of the heavy metal content in the leaching solutions.

	Set No.			USEPA limits [mg.L^{-1}]
	B [mg.L^{-1}]	D [mg.L^{-1}]	I [mg.L^{-1}]	
Al	129.94	75.27	78.8	-
Cd	0.00	0.00	0.00	1
Cr	0.40	0.27	0.29	5
Cu	0.14	0.10	0.10	-
Fe	112.74	71.77	75.54	-
Na	37.06	26.68	26.47	40
Ni	0.03	0.00	0.00	-
Pb	0.00	0.00	0.00	5

3.2. Analysis of Data Using the Multi-Response Optimization Grey-Based Taguchi Method

The following sections discuss the effect of varied weight percentages of red mud and silica fume. The study evaluates compressive strength and water absorption across various brick sets using a multi-response optimization Grey-based Taguchi method. Data from the orthogonal array experiments were analyzed with MINITAB Release 19 software. In this

Table 8: S/N ratio, normalised S/N ratio and absolute difference.

Set No.	S/N ratio		Normalized value of S/N ratios Z_{ij}		Absolute difference [Δ_{ij}]	
	S/N (Compressive Strength)	S/N (Water Absorption)	Z (Compressive Strength)	Z (Water Absorption)	Δ (Compressive strength)	Δ (Water Absorption)
A	10.51	-21.72	0.42	0.00	0.58	1.00
B	13.92	-23.71	0.99	1.00	0.01	0.00
C	12.52	-23.34	0.76	0.82	0.24	0.18
D	11	-22.72	0.50	0.50	0.50	0.50
E	9.81	-21.72	0.30	1.00	0.70	0.00
F	10.60	-21.71	0.44	0.00	0.56	1.00
G	8.00	-22.01	0.00	0.15	1.00	0.85
H	9.89	-22.89	0.32	0.59	0.68	0.41
I	10.48	-22.43	0.42	0.36	0.58	0.64

Table 9: Grey Relational coefficient and Grey Relational Grade.

Set No.	Grey Relational coefficient (GC)		Grey relational grade
	GC (Compressive Strength)	GC (Water Absorption)	GRG
A	0.56	0.20	0.383
B	0.99	1.00	0.997
C	0.76	0.57	0.666
D	0.60	0.34	0.469
E	0.52	1.00	0.758
F	0.57	0.20	0.386
G	0.43	0.23	0.328
H	0.52	0.38	0.451
I	0.56	0.28	0.422

work, compressive strength is considered a 'the larger the better' characteristic, as the goal is to maximize strength; therefore, Equation 1 from section 2.2.3 was used to calculate the S/N ratio for compressive strength. Water absorption, on the other hand, is a 'the smaller the better' trait, since it should be minimized; hence, Equation 2 was employed to determine the S/N ratio for water absorption. The results, including S/N ratios, normalized S/N ratios, and absolute differences per experiment, are summarized in Table 8.

The statistics of Table 8 are used to determine the grey relational coefficient using equation 6 of section 2.2.3, as demonstrated in Table 9.

The value for λ is between 0 and 1, depending on the process parameter weightage.

Finally, the GRG from equation 7 and the estimation model for the GRG were determined in this way,

GRG = 0.5398 + 0.1420 RM_13.75 - 0.0024 RM_18.79 - 0.1396 RM_23.79 - 0.1466 SF_5 + 0.1953 SF_10 - 0.0487 SF_15 + 0.0441 WFS_7.85 + 0.0892 WFS_12.85 - 0.1334 WFS_17.85

Table 10: Optimum Conditions.

	Optimum conditions using GRG		
	RM	SF	WFS
Level 1	0.682	0.393	0.584
Level 2	0.537	0.735	0.629
Level 3	0.400	0.491	0.406
Rank	2	1	3

Table 11: Main effects on grey grades.

Factors	Levels			For each factor-level
	1	2	3	SS_T
RM	0.682	0.537	0.400	0.119
SF	0.393	0.735	0.491	0.186
WFS	0.584	0.629	0.406	0.083

The factors for optimization are outlined in Table 10. The optimal parameter conditions (RM1SF2WFS2) were identified based on the highest GRG in Table 11. These conditions agree with experimental Set B, as presented in Table 3. Among the factors, SF exhibited the steepest slope, followed by RM and WFS, as shown in Fig. 7. To achieve maximum compressive strength, the levels 1, 2, and 2 are ideal for SF, WFS, and RM, respectively. This finding is also consistent with the criteria corresponding to the highest GRG value in Table 11.

The main impacts of the process parameters on the mean response were also investigated using the GRG value. The average value of the quality characteristic for each factor at various levels is called the "mean response".

Table 11 presents the average GRG values for each factor at the three different levels. The response analysis confirms that the optimal parameters are levels 1, 2, and 2 for RM, SF, and WFS, respectively (Fig. 7). Figure 7 illustrates the mean GRG values for compressive strength and water absorption of red mud-based geopolymeric bricks across

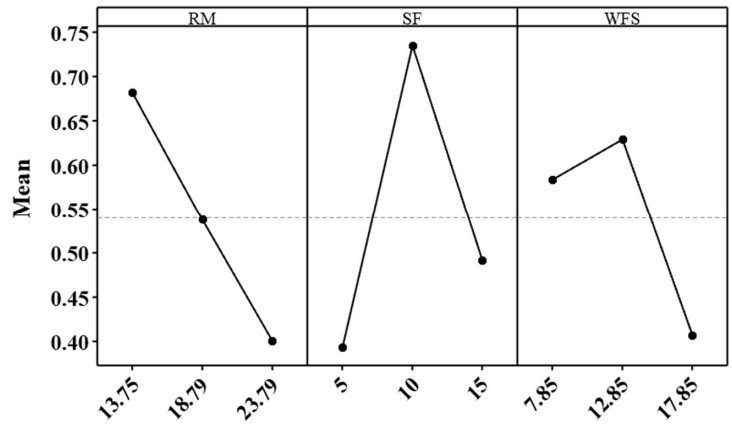

Fig. 7: Main Effect Plot of GRG.

various parameter levels, namely RM (%), SF (%), and WFS (%). The data show that increasing the RM percentage from 13.75% to 23.79% results in a decrease in the mean GRG values for both compressive strength and water absorption. This decline at higher RM concentrations occurs because increased Fe_2O_3 content inhibits fly ash interaction, leading to reduced aluminosilicate gel formation. Conversely, increasing the SF content from 5% to 10% causes the GRG values to rise, with the improvement in compressive strength attributed to the higher amorphous SiO_2 content in silica fume. As SF increases from 5% to 10%, the Si/Al ratio also rises, promoting the formation of N-A-S-H gel during geopolymerization. Additionally, the GRG value increases as WFS decreases from 17.85% to 12.85% (Bajpai et al. 2020). Parallel lines in an interaction plot indicate no interaction between variables. In contrast, a departure from the parallel state indicates that interaction exists between the variables being studied. The mutual dependence between the variables increases with the degree of deviation from the parallel state (Montes & Allouche 2012).

The interaction plot (Fig. 8) shows that all lines intersect, indicating a significant relationship between the components and the GRG value, as evidenced by the non-parallel lines in the interaction map. In the first row of the two graphs, at 13.75% RM, SF and WFS markedly influenced the GRG value. However, when RM increased to 18.79%, the impact of SF and WFS on the GRG value diminished. At 23.99% RM, SF and WFS showed no observable effect on the GRG value. This is likely because the finer RM crystallized on the exterior of the coarser particles, possibly preventing the coarser particles from participating in further reactions, which explains why SF and WFS did not influence the GRG value at this higher RM percentage (Bajpai et al. 2020).

In the second row of the graph, when the weight percentage of SF increased from 5% to 10%, the impact of RM and WFS increased, but it decreased at 15% SF. The graphs in all three rows show that the maximum GRG value appears at RM level 1, SF level 2, and WFS level 2.

The three-dimensional surface plot showing the effects of the three parameters on GRG is presented in Fig. 9(a). The plot indicates that SF affected the GRG value more significantly than RM. Red mud acts as a filler in the geopolymer matrix, enhancing the compressive strength of the bricks at a replacement level of 13.75%. When the percentage of red mud increased beyond 13.75%, it hindered the geopolymer reaction and reduced the compressive strength of the bricks. Similar results were reported in earlier research (Singh et al. 2020). The GRG value was higher at 12.85% WFS and decreased as the percentage of SF increased from 10% to 15%, as shown in Fig. 9(b). SF had a greater influence on the GRG value compared to the percentage of WFS. Fig. 9(c) shows that the GRG value was maximum at 10% SF and 12.85% RM.

The importance of process parameters was examined using ANOVA. An ANOVA was conducted with the GRG value to identify key factors. The results are shown in Table 12. RM, SF, and WFS emerged as significant parameters affecting GRG, with p-values less than 0.005 at a 95% confidence level. Additionally, each factor notably influences compressive strength, as detailed in Table 12, which presents the F-ratio and contribution percentages

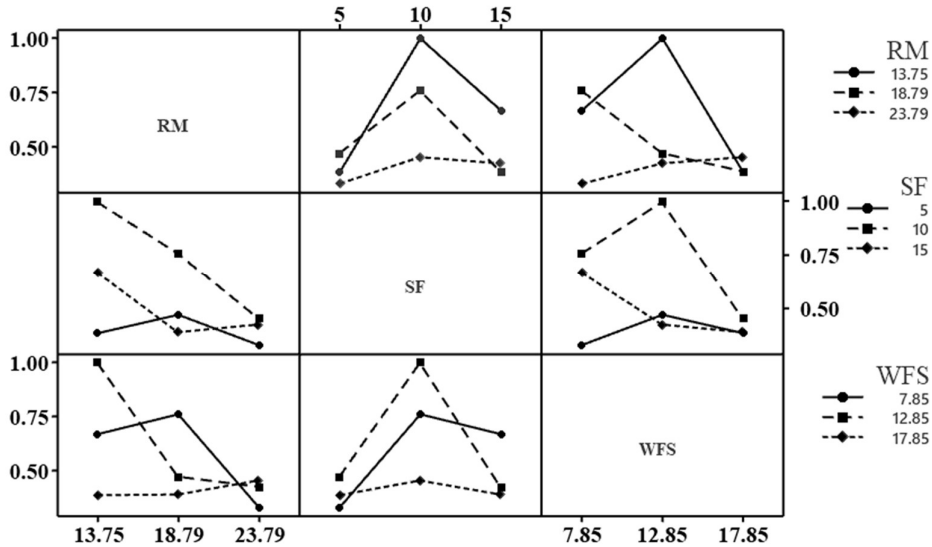

Fig. 8: Interaction plot for GRG.

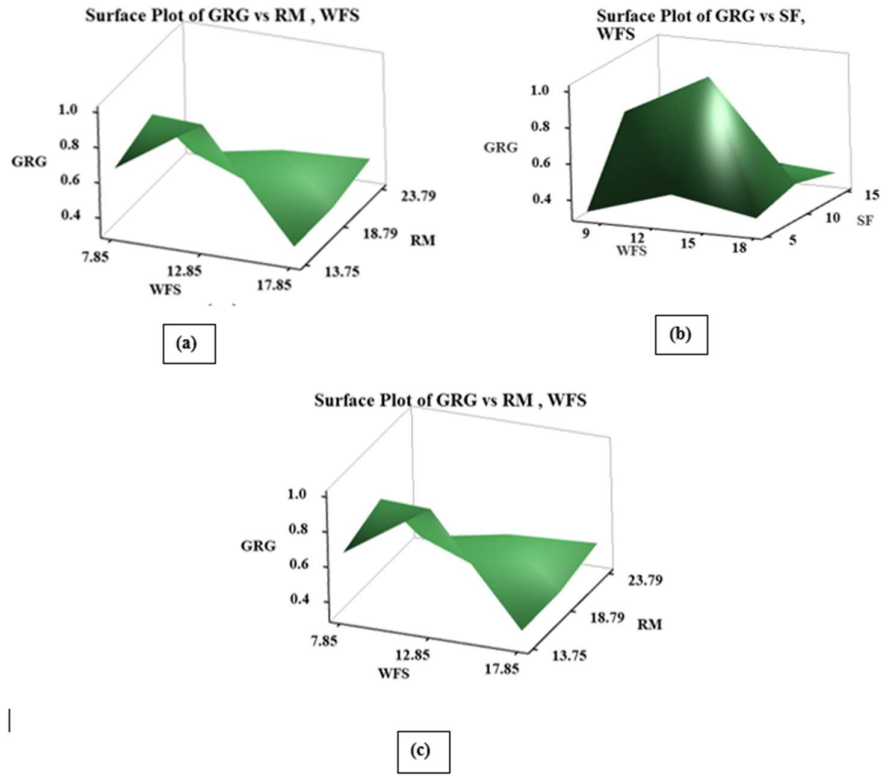

Fig. 9: Surface plot: (a) The influence of SF and RM on GRG, (b) The influence of WFS and SF on GRG, (c) The influence of WFS and RM on GRG.

Table 12: Results of ANOVA on grey grade.

Factor	SS_T	DOF	V	F	P	%CF	Conclusion
RM	0.119	2	0.059	28.14	0.034	30.36	Significant
SF	0.186	2	0.093	43.99	0.022	47.45	Significant
WFS	0.083	2	0.0415	19.64	0.048	21.17	Significant
Error	0.004	2	0.002	----	----	1.02	----
Total	0.392	8	----				

for each parameter. Notably, SF had a substantial impact on the response, indicated by its high F-ratio of 43.39. The ANOVA results clearly indicate that the primary contributors to the compressive strength and water absorption of cast geopolymeric bricks are 47.45% silica fume, followed by 30.36% red mud and 21.17% WFS. In the geopolymerization process, alkalinity is crucial. In this study, red mud-based geopolymeric bricks were prepared by partially replacing clay with varying percentages of RM, SF, and WFS, using an alkaline activator. The red mud used contains 5.89% (w/w) Na2O (bound caustic). The highest compressive strength of 5 N.mm^{2-} was achieved with 10% SF and 13.75% RM, due to increased alkalinity from RM. Strength decreased as RM and SF percentages increased because higher RM levels raise alkalinity, accelerating alumina dissolution from materials like RM, FA, and SF, which then act as fillers and inhibit the geopolymerization process (Shivaprasad & Das 2018, Singh et al. 2020).

Fig. 10 displays the normal probability plot of the GRG residual, which exhibits a straight line, indicating the effectiveness of this model.

The final stage of grey relational analysis involves predicting and verifying the performance improvement of responses once the optimal factors have been identified. The predicted GRE was calculated using equation 11. To validate these findings, confirmation tests were conducted, and the average GRE from three runs was determined. Additionally, Table 13 shows that the results of the confirmation experiments are consistent with the predicted values.

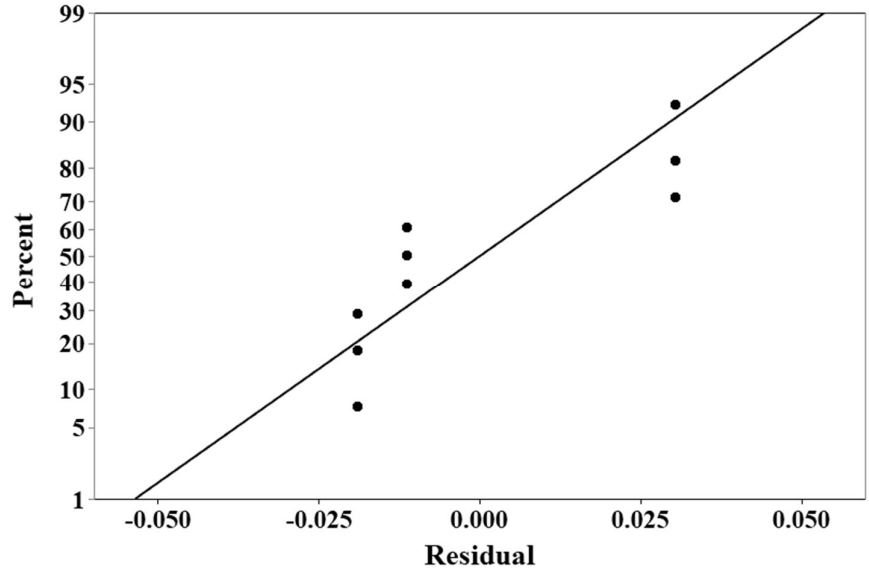

Fig. 10: Normal probability plot of residuals for GRG.

Table 13: Results of the confirmation experiment.

	Optimal Design Parameters	
	Prediction	Experiment
Optimal Factors Level	RM1 SF2 WFS2	RM1 SF2 WFS2
GRG	0.967	0.997

$$\text{GRG predicted} = GRG_m + \sum_{i=1}^{q} GRG_o - GRG_m \quad \ldots(11)$$

Where denotes the maximum of the average at the optimal level of factors GRG and reparents mean GRG. Number of factors represented by q.

4. CONCLUSIONS

Higher compressive strength was observed in set B, due to the formation of a continuous and denser inorganic polymer compared to set D. Unreacted silicon dioxide and aluminum oxide from fly ash and RM are integrated into the geopolymer gel, leading to a more uniform and solid structure. During geopolymerization, aluminosilicate gel plays a vital role in immobilizing metallic species through mineral encapsulation, ion exchange, and physical entrapment within a highly cross-linked aluminosilicate network. The dense structure and stable Si–O–Al bonds reduce metal mobility by decreasing pore connectivity and leachable phases. The highest compressive strength of 5.02 $N.mm^{-2}$ in set B was achieved with optimal proportions of red mud, silica fume, and fresh caustic concentration. Leachability tests confirmed that the bricks contain trace elements well below USEPA limits, ensuring environmental safety. Future work should focus on cost optimization and long-term durability evaluation of these geopolymers. This study aimed to maximize compressive strength using a 5M total caustic concentration in clay bricks with an optimized mix of red mud, Desur clay, silica fume, and caustic soda, along with WFS and fly ash. The optimal proportions were 13.17% red mud (level 1), 10% silica fume (level 2), and 12.85% based on GRG. ANOVA results indicated that silica fume contributed the most (47.45%) to the response, followed by red mud (30.36%), with WFS contributing the least (21.17%). These optimal conditions aligned with experimental set B. Additionally, future research should include long-term durability and leachability assessments through aging tests such as prolonged water immersion, cyclic wetting–drying, and exposure to weak acids to evaluate the potential release of metals under aggressive environmental conditions.

5. ACKNOWLEDGEMENT

The authors are grateful to the Department of Civil Engineering, KLE Technological University, M. S. Sheshgiri Campus, Belagavi, for providing the necessary institutional facilities. The authors would also like to thank Kolhapur Institute of Technology's College of Engineering (Autonomous), Kolhapur, India, for permitting us to perform laboratory work. The red mud used in this work was supplied by HINDALCO Industries Ltd., Belgaum, Karnataka, India, and is greatly acknowledged. The authors greatly appreciate the help of the Physics Department, Shivaji University, Kolhapur, Maharashtra, for SEM analysis. The authors also acknowledge the Common Facility Center, Shivaji University, Kolhapur, for providing XRD and TCLP analysis facilities.

6. REFERENCES

Abbas, S., Saleem, M.A., Kazmi, S.M.S., and Munir, M.J., 2017. Production of sustainable clay bricks using waste fly ash: Mechanical and durability properties. *Journal of Building Engineering*, 14, pp.7-14. [DOI]

Apithanyasai, S., Supakata, N., and Papong, S., 2020. The potential of industrial waste: using foundry sand with fly ash and electric arc furnace slag for geopolymer brick production. *Heliyon*, 6(3), pp.e03697. [DOI]

Bajpai, R., Shrivastava, A., and Singh, M., 2020. Properties of fly ash geopolymer modified with red mud and silica fume: a comparative study. *SN Applied Sciences*, 2(11), pp.1846. [DOI]

Billong, N., Oti, J., and Kinuthia, J., 2021. Using silica fume based activator in sustainable geopolymer binder for building application. *Construction and Building Materials*, 275, pp.e122177. [DOI]

Dass, A. and Malhotra, S.K., 1990. Lime-stabilized red mud bricks. *Materials and Structures*, 23, pp.252-255. [DOI]

Duxson, P., Mallicoat, S.W., Lukey, G.C., Kriven, W.M., and van Deventer, J.S.J., 2007. The effect of alkali and Si/Al ratio on the development of mechanical properties of metakaolin-based geopolymers. *Colloids and Surfaces A: Physicochemical and Engineering Aspects*, 292(1), pp.8-20. [DOI]

Gaonkar, P.V., Bevinakatti, S., Hoolikantimath, N.P., Borchate, S.S., Katageri, B.G., and Ghorpade, P.A., 2023. A geopolymeric approach to utilize the bound caustic of Bayer's red mud and waste foundry sand in clay brick. *Indian Geotechnical Journal*, 53(2), pp.473-483. [DOI]

Hafez, R.D.A., Tayeh, B.A., and Abd-Al Ftah, R.O., 2022. Development and evaluation of green fired clay bricks using industrial and agricultural wastes. *Case Studies in Construction Materials*, 17, pp.e01391. [DOI]

Ishaq, M., Ali, A., Hussain, A.A., Kamran, K., Ghuffar, A., and Anwar, A., 2025. Industrial waste as clay substitute in brick manufacturing. *Construction and Building Materials*, 477, pp.141359. [DOI]

Jozanikohan, G. and Abarghooei, M.N., 2022. The Fourier transform infrared spectroscopy (FTIR) analysis for the clay mineralogy studies in a clastic reservoir. *Journal of Petroleum Exploration and Production Technology*, 12(8), pp.2093-2106. [DOI]

Kumar, A. and Kumar, S., 2013. Development of paving blocks from synergistic use of red mud and fly ash using geopolymerization. *Construction and Building Materials*, 38, pp.865-871. [DOI]

Kumar, A., Saravanan, T.J., Bisht, K., and Kabeer, K.I.S.A., 2021. A review on the utilization of red mud for the production of geopolymer and alkali activated concrete. *Construction and Building Materials*, 302, pp.187-192. [DOI]

Kumar, S., Ansari, M.A., Kant, L., and Nand, N., 2025. An experimental investigation on sustainable concrete made with refractory brick as a substitute of natural fine aggregate. *Nature Environment and Pollution Technology*, 24(1), pp.B4202. [DOI]

Matos, P.R. de, Marcon, M.F., Schankoski, R.A., and Prudêncio, L.R., 2019. Novel applications of waste foundry sand in conventional and dry-mix concretes. *Journal of Environmental Management*, 244, pp.294-303. [DOI]

Mohmed, A. and Scholar, A.B., 2018. Studies on the role of silica fume in geopolymer concrete and its properties. *International Journal of Civil Engineering and Technology (IJCIET)*, 9(7), pp.112-122.

Montes, C. and Allouche, E., 2012. Influence of activator solution formulation on fresh and hardened properties of low-calcium fly ash geopolymer concrete. *Coal Combustion and Gasification Products*, 4(1), pp.1-9. [DOI]

Mudgal, M., Singh, A., Chouhan, R.K., Acharya, A., and Srivastava, A.K., 2021. Fly ash red mud geopolymer with improved mechanical strength. *Cleaner Engineering and Technology*, 4, pp.100215. [DOI]

Nandipati, S., Srinivasa Rao, G.V.R., Manjunatha, M., Dora, N., and Bahij, S., 2023. Potential use of sustainable industrial waste byproducts in fired and unfired brick production. *Advances in Civil Engineering*, 2023, pp.9989054. [DOI]

Ogundiran, M.B. and Kumar, S., 2015. Synthesis and characterisation of geopolymer from Nigerian clay. *Applied Clay Science*, 108, pp.173-181. [DOI]

Phoo-ngernkham, T., Chindaprasirt, P., Sata, V., Hanjitsuwan, S., and Hatanaka, S., 2014. The effect of adding nano-SiO2 and nano-Al2O3 on properties of high calcium fly ash geopolymer cured at ambient temperature. *Materials and Design*, 55, pp.58-65. [DOI]

Rai, S., Bahadure, S., Chaddha, M.J., and Agnihotri, A., 2020. Disposal practices and utilization of red mud (bauxite residue): a review in Indian context and abroad. *Journal of Sustainable Metallurgy*, 6(1), pp.1-8. [DOI]

Rai, S., Wasewar, K.L., Lataye, D.H., Mishra, R.S., Puttewar, S.P., Chaddha, M.J., Mahindiran, P., and Mukhopadhyay, J., 2012. Neutralization of red mud with pickling waste liquor using Taguchi's design of experimental methodology. *Waste Management and Research*, 30(9), pp.922-930. [DOI]

Rajesrajeswari, A., Dhinakaran, G., and Mohamed, E., 2014. Compressive strength of silica fume based geopolymer concrete. *Asian Journal of Applied Science*, 7(4), pp.240-247. [DOI]

Reddy, P.S., Reddy, N.G., Serjun, V.Z., Mohanty, B., Das, S.K., Reddy, K.R., and Rao, B.H., 2021. Properties and assessment of applications of red mud (bauxite residue): current status and research needs. *Waste and Biomass Valorization*, 12(3), pp.1185-1217. [DOI]

Saravanan, J. and Rao, P.V., 2023. Past investigations on development of sustainable bricks – a comprehensive review. *Sustainable Chemistry for the Environment*, 3, pp.100030. [DOI]

Shill, S.K., Al-Deen, S., Ashraf, M., and Hutchison, W., 2020. Resistance of fly ash based geopolymer mortar to both chemicals and high thermal cycles simultaneously. *Construction and Building Materials*, 239, pp.117886. [DOI]

Shivaprasad, K.N. and Das, B.B., 2018. Determination of optimized geopolymerization factors on the properties of pelletized fly ash aggregates. *Construction and Building Materials*, 163, pp.428-437. [DOI]

Siddique, R. and Chahal, N., 2011. Use of silicon and ferrosilicon industry by-products (silica fume) in cement paste and mortar. *Resources, Conservation and Recycling*, 55(8), pp.739-744. [DOI]

Singh, S., Aswath, M.U., and Ranganath, R.V., 2020. Performance assessment of bricks and prisms: red mud based geopolymer composite. *Journal of Building Engineering*, 32(3), pp.101462. [DOI]

Sontia Metekong, J.V., Kaze, C.R., Kamseu, E., Chinje, F.U., and Tatietse, T.T., 2024. Feasibility of production fired bricks based lateritic soil at very low temperature. *International Journal of Ceramic Engineering and Science*, 6(4), pp.e10225. [DOI]

Sutar, H., Mishra, S.C., Sahoo, S.K., Chakraverty, A.P., and Maharana, H.S., 2014. Progress of red mud utilization: an overview. *American Chemical Science*, 4(3), pp.255-279. [DOI]

Toniolo, N., Taveri, G., Hurle, K., Roether, J.A., Ercole, P., Dlouhý, I., and Boccaccini, A.R., 2017. Fly-ash-based geopolymers: how the addition of recycled glass or red mud waste influences the structural and mechanical properties. *Journal of Ceramic Science and Technology*, 8(3), pp.411-419. [DOI]

Turkey, F.A., Beddu, S.B., Ahmed, A.N., and Al-Hubboubi, S.K., 2022. Effect of high temperatures on the properties of lightweight geopolymer concrete based fly ash and glass powder mixtures. *Case Studies in Construction Materials*, 17, pp.e01489. [DOI]